



# Cohesive zone finite element analysis of crack initiation from a butt joint's interface corner



E.D. Reedy Jr.

Sandia National Laboratories, Albuquerque, NM 87185, USA

## ARTICLE INFO

### Article history:

Received 14 February 2014

Received in revised form 13 August 2014

Available online 6 September 2014

### Keywords:

Cohesive zone

Bonded joint

Interface corner

Interfacial fracture

## ABSTRACT

Cohesive zone (CZ) fracture analysis techniques are used to predict the initiation of crack growth from the interface corner of an adhesively bonded butt joint. In this plane strain analysis, a thin linear elastic adhesive layer is sandwiched between rigid adherends. There is no preexisting crack in the problem analyzed, and the focus is on how the shape of the traction–separation ( $T$ – $U$ ) relationship affects the predicted joint strength. Unlike the case of a preexisting interfacial crack, the calculated results clearly indicate that the predicted joint strength depends on the shape of the  $T$ – $U$  relationship. Most of the calculations used a rectangular  $T$ – $U$  relationship whose shape (aspect ratio) is defined by two parameters: the interfacial strength  $\sigma^*$  and the work of separation/unit area  $\Gamma$ . The principal finding of this study is that for a specified adhesive layer thickness, there is any number of  $\sigma^*$ ,  $\Gamma$  combinations that generate the same predicted joint strength. Each combination corresponds to a different CZ length. An approximate CZ-like elasticity solution was developed to show how such combinations arise and their connection with the CZ length.

© 2014 Elsevier Ltd. All rights reserved.

## 1. Introduction

The cohesive zone (CZ) fracture modeling technique is now commonly used to predict failure of bodies containing an initial crack (Tvergaard and Hutchinson, 1993; Xu and Needleman, 1994) and adhesively bonded joints (Yang and Thouless, 2001; Kafkalidis and Thouless, 2002; Blackman et al., 2003; Liljedahl et al., 2006; Banea and da Silva, 2009; Gustafson and Waas, 2009). When used in an analysis where all bulk materials are linear elastic, one recovers linear elastic fracture mechanics predictions provided that the CZ is sufficiently small when compared to the crack length (i.e., similar to a small-scale yielding requirement). Even though the shape of the traction–separation ( $T$ – $U$ ) relationship used in a CZ fracture analysis affects the length of the CZ, this change in length has negligible effect if the CZ is sufficiently small. In such cases the solution only depends on the area under the  $T$ – $U$  relationship, which equals the work of separation/unit area of crack advance (i.e., fracture toughness).

Although most frequently applied to cracked bodies, a CZ failure analysis has also been applied with some success to problems where there is no preexisting crack, but where failure initiates from sharp discontinuities such as generated by corners or sharp notches. For example, CZ modeling techniques have been applied

to V-notched PMMA samples with various notch angles, depths, and sizes (Gomez and Elices, 2003). In this study, the specimens were loaded either in tension or bending. Predicted strengths were generally in good agreement with the experimental results. These authors indicated that they found that the rectangular  $T$ – $U$  relationship was the best shape to reproduce all experimental results. The reason why this is true was not discussed. In another study, a CZ analysis was used to predict the initiation of crack growth from the bimaterial corner of an aluminum/epoxy specimen (Mohammed and Liechti, 2000). In this work, a CZ model was calibrated using experimental data for an interfacial crack and then used to successfully predict the strength of specimens with varying corner angles. The present work examines the use of a CZ fracture analysis to predict the strength of a sharp-edged, adhesively bonded butt joint. This type of joint is commonly used to evaluate adhesives and is also a relatively simple geometry to analyze.

## 2. Failure analysis of an adhesively bonded butt joint based on a critical value of the interface corner stress intensity factor

In previous work, a method analogous to traditional fracture mechanics was found to accurately predict the strength of sharp-edged, adhesively bonded butt joints (Reedy, 1990; Reedy and Guess, 1993, 1997, 1999). This technique uses the stress intensity factor associated with the interface corner (IC) discontinuity

E-mail address: [edreedy@sandia.gov](mailto:edreedy@sandia.gov)

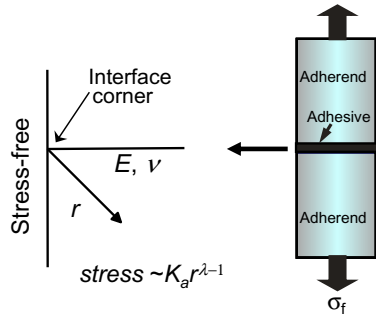


**Fig. 1.** Adhesively bonded, sharp-edged cylindrical butt joint with the associated idealized plane strain asymptotic problem of an elastic quarter-plane bonded to a rigid quarter-plane.

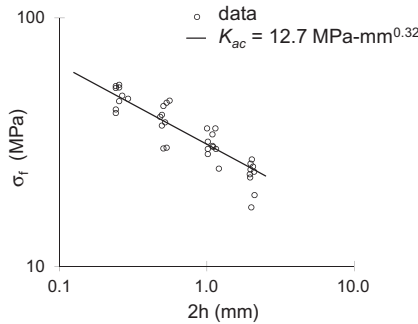


**Fig. 2.** Comparison of measured butt joint tensile strength vs. bond thickness data with prediction based on an interface corner toughness of 12.7 MPa-mm<sup>0.32</sup>.

(Fig. 1). The stress state in the region of the IC varies as  $K_a r^{\lambda-1}$  where  $r$  is the distance from the IC and  $\lambda - 1$  is the order of the power-law singularity (which is weaker than that found at a crack tip). The value of the IC stress intensity factor  $K_a$  determines the magnitude of the stress state in the region of the interface corner. It depends on loading, geometry, and layer elastic properties. For a thin adhesive layer sandwiched between rigid adherends

$$K_a = \frac{\nu}{1-\nu} \sigma_n h^{1-\lambda} A(\nu) \quad (1)$$

where  $A(\nu)$  is a function of Poisson's ratio  $\nu$ ,  $2h$  is the thickness of the adhesive layer, and  $\sigma_n$  is the nominal applied tensile stress (applied load/cross sectional area). The strength of the singularity also depends on  $\nu$ . When  $\nu = 0.35$ ,  $A(\nu) = 0.958$ , and  $1 - \lambda = 0.320$ .

The IC failure theory for adhesively bonded butt joints postulates that fracture initiates once the surrounding stress field reaches a critical state

$$K_a \text{ (loading)} = K_{ac} \text{ (material property)} \quad (2)$$

where the critical value of the IC stress intensity factor  $K_{ac}$  is a measured material property and is referred to as the IC toughness. This approach requires that the asymptotic stress state characterized by  $K_a$  must dominate a region about the interface corner that is significantly larger than the fracture process zone, intrinsic flaw size, and the plastic yield zone (i.e., requirements similar to small scale yielding in linear elastic fracture mechanics). This technique was found to accurately predict the observed variation in joint strength with bond thickness. If  $K_a$  is equal to  $K_{ac}$ , then Eq. (1) requires  $\sigma_f h^{1-\lambda}$  to remain constant, where  $\sigma_f$  is the nominal butt joint tensile strength (failure load/cross sectional area). The measured tensile strength of butt joints formed by bonding 28.6-mm diameter, stainless steel adherends together with an epoxy adhesive was found to follow the predicted power-law relationship between joint strength and

bond thickness as shown in Fig. 2. A detailed description of the butt joint tests that measured the strength data plotted in Fig. 2 is documented elsewhere (Reedy and Guess, 1993). Note that in these tests the plastic yield zone emanating from the interface corner is estimated to be less than 2% of the bond thickness, and consequently, the small scale yielding idealization applies. Similar levels of agreement with butt joint strength data have been observed for other butt joint tests (Reedy and Guess, 1997, 1999). One of the questions being addressed in this study is whether a CZ failure analysis could provide an alternate approach for predicting the strength of adhesively bonded butt joints.

### 3. CZ Fracture analysis of an adhesively bonded butt joint

In a CZ model, interfacial separation is defined in terms of an effective interfacial traction vs. separation relationship (Fig. 3). Key parameters defining this  $T$ - $U$  relationship are the interfacial strength  $\sigma^*$  and the work of separation/unit area  $\Gamma$ . A CZ separation model is computationally attractive for simulating interfacial failure since crack growth is a natural outcome of the solution, and moreover it leads to mesh-independent results since a length scale is embedded within the model (provided that the mesh is fine enough to resolve the CZ – the region of interfacial softening behind the crack tip). The particular CZ formulation used in this study is similar to that used by Tvergaard and Hutchinson (1993). The effective separation  $\chi$  is defined as

$$\chi = \sqrt{\left(\frac{\delta_n}{\delta_n^c}\right)^2 + \left(\frac{\delta_t}{\delta_t^c}\right)^2} \quad (3)$$

where  $\delta_n$  and  $\delta_t$  are the normal and tangential displacement jump across the interface while  $\delta_n^c$  and  $\delta_t^c$  are the respective critical values. Since there is no compelling reason to assume otherwise,  $\delta_n^c = \delta_t^c = \delta_c$  is assumed. The normal and tangential interfacial tractions ( $T_n$  and  $T_t$ , respectively) are defined via the potential

$$\phi(\delta_n, \delta_t) = \delta_c \int_0^\chi \sigma(\chi') d\chi' \quad (4)$$

with

$$T_n = \frac{\partial \phi}{\partial \delta_n} = \frac{\sigma(\chi)}{\chi} \frac{\delta_n}{\delta_c} \quad \text{and} \quad T_t = \frac{\partial \phi}{\partial \delta_t} = \frac{\sigma(\chi)}{\chi} \frac{\delta_t}{\delta_c} \quad (5)$$

Normal interpenetration is penalized by applying a prescribed multiple of the initial loading stiffness. Unless indicated otherwise, a trapezoidal  $T$ - $U$  relationship was used, where  $\chi_1$  and  $\chi_2$  define its shape. The trapezoidal  $T$ - $U$  relationship was chosen for its simplicity and a relationship with steep loading and unloading slopes was used ( $\chi_1 = 0.01$  and  $\chi_2 = 0.99$ ). Consequently, the shape of the  $T$ - $U$  relationship is essentially rectangular and will be referred to as such. The work of separation per unit area of interface (i.e., intrinsic interfacial toughness) is path independent and equals the value of the potential  $\phi$  evaluated at  $\chi = 1$  (Eq. (4)). For the assumed

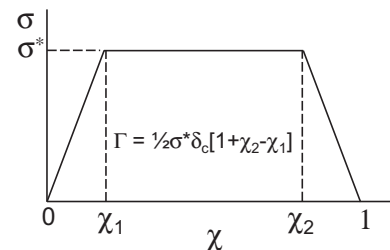


**Fig. 3.** Effective  $T$ - $U$  relationship used in conjunction with the CZ model (in this study  $\chi_1 = 0.01$  and  $\chi_2 = 0.99$ , and the  $T$ - $U$  is approximately rectangular).

trapezoidal relationship, the toughness  $\Gamma = \frac{1}{2}\sigma^*\delta_c[1 + \chi_2 - \chi_1]$  (i.e., 99% of that of a rectangular  $T$ - $U$  relationship when  $\chi_1 = 0.01$  and  $\chi_2 = 0.99$ ). The length of the CZ  $L_{CZ}$  is defined as the region of interfacial softening where  $\chi_1 < \chi < 1$  (i.e., if considered rectangular, where  $\sigma = \sigma^*$ ).

In the work reported herein, an idealization of the butt joint geometry that was tested in previous work is analyzed (Figs. 1 and 2). In those tests, cylindrical, stainless steel adherends were bonded together with an epoxy adhesive (Reedy and Guess, 1993). Since the steel adherends are much stiffer than the epoxy adhesive layer, the adherends can be considered rigid. Furthermore, the bond length can be considered to be semi-infinite since the thickness of the adhesive layer is much smaller than any other joint dimension. Estimates for the extent of epoxy yielding in the tested butt joints indicate that small scale yielding occurred. Accordingly, the adhesive layer was modeled as linear elastic and the joint is idealized as a thin, linear elastic adhesive layer sandwiched between rigid adherends (Fig. 4). All material nonlinearity is incorporated in the cohesive zone model. The layer has thickness  $2h$  and length  $2L$ , and in all calculations  $L/h = 40$  so as to closely approximate an infinitely long bond (symmetry condition were applied so that only one-half of the layer length is modeled). In this plane strain analysis, the bottom edge of the elastic layer is fixed while the top edge is displaced upward. Note that although this is a plane strain analysis, axisymmetric calculations will yield similar results for sufficiently large  $L/h$  since the rigid adherends limit radial displacements (Reedy, 1990). In the results reported here, the elastic layer has a Young's modulus  $E = 3.5$  GPa, Poisson's ratio  $\nu = 0.35$ , and its thickness  $2h = 0.5$  mm (unless indicated otherwise). Interfacial separation is presumed to occur only along the upper interface (in the butt joint tests, failure always initiated on one interface along a small segment of the specimen periphery (Reedy and Guess, 1993)). The finite element mesh is highly refined in the region surrounding the upper interface corner and cohesive surface elements are pre-inserted along the interface in this region. The normalized characteristic element length  $\Delta/h$  in the refined region is either 0.002 or 0.004 (smaller CZ elements are used when the choice of problem parameters generate a relatively small CZ) and the refined area was  $50\Delta$  by  $50\Delta$  or larger. Test calculations comparing results for  $\Delta/h = 0.002$  and  $\Delta/h = 0.004$  generated essentially the same predicted failure loads (within 1%, see Table 1). Sandia National Laboratories' Sierra/SM implicit quasistatics finite element code was used to perform the analysis (Thomas, 2011).

#### 4. Effect of varying the $\Gamma$ , $\sigma^*$ values that define a rectangular $T$ - $U$ relationship

The sensitivity of the predicted butt joint tensile strength to the shape (aspect ratio) of the rectangular  $T$ - $U$  relationship used in the CZ analysis was investigated. Fig. 5 plots the  $T$ - $U$  relationships that were used in the analysis. The work of separation per unit area of interface was held fixed a  $20 \text{ J/m}^2$  while the interfacial strength  $\sigma^*$  was varied from 60 to 100 MPa. The calculated butt joint tensile

**Table 1**

Predicted joint strength when a rectangular (rect)  $T$ - $U$  relationship is used is compared to that predicted when a triangular (tri)  $T$ - $U$  relationship is used where both relationships have the same value of  $\Gamma$  and  $\sigma^*$  ( $\sigma^* = 80 \text{ MPa}$ , and  $\Gamma = 20 \text{ J/m}^2$ ). Results for two levels of mesh refinement.

$2h$ (mm)	$\Delta$ (mm)	Type $T$ - $U$	$\sigma_f$ (MPa)	$L_{CZ}$ (mm)	$K_a$ MPa-mm <sup>0.32</sup>
0.5	0.0010	rect	48.4	0.015	16.0
0.5	0.0005	rect	48.1	0.015	15.9
0.5	0.0010	tri	39.6	0.014	13.1
0.5	0.0005	tri	39.6	0.015	13.1

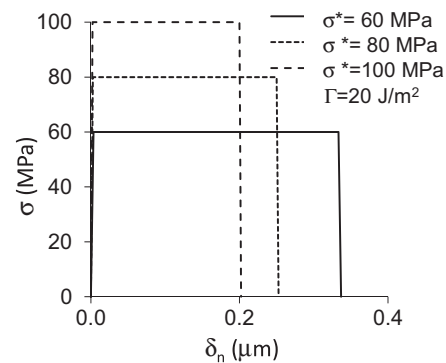


**Fig. 5.**  $T$ - $U$  relationships used in calculations where  $\Gamma$  is held fixed while  $\sigma^*$  is varied (curves for case of a pure mode I loading).

strength  $\sigma_f$  is defined as the normal stress at the center of the layer when the crack first begins to propagate (i.e., the magnitude of the tensile stress in a region far from the interface corner where the layer stress is uniform). The CZ is fully developed at this point, and any further increase in load would cause the crack to propagate rapidly. Fig. 6 shows that the predicted joint strength varies with the value of  $\sigma^*$  even though  $\Gamma$  is fixed. As shown in Fig. 7, the length of the CZ  $L_{CZ}$  also varies with  $\sigma^*$ . In these calculations,  $L_{CZ}$  is small relative to the layer thickness. Previous work has shown that the interface corner singularity dominates a region that extends to  $\sim 0.3h$  (when  $\nu = 0.35$ – $0.4$ ), and so small scale yielding conditions apply (Reedy, 1993, 2000). This result can be contrasted with CZ predictions for a long interfacial crack between elastic materials. In the long crack case the predicted strength will be independent of the shape of the CZ model used in the analysis and the predicted strength will agree with a linear elastic fracture mechanics prediction (provided that the CZ length is small compared to all problem dimensions including crack length). In analyses where there is no preexisting crack, the CZ could be considered to be the “initial flaw” and, consequently, its length as well as the magnitude and distribution of CZ tractions would matter. Since  $L_{CZ}$  and CZ tractions depend on the details of the  $T$ - $U$  relationship, one might anticipate that the predicted joint strength will also depend on the shape of the  $T$ - $U$  relationship.

Since the predicted butt joint strength depends on both  $\Gamma$  and  $\sigma^*$ , it seems likely that there may be any number of  $\Gamma$ ,  $\sigma^*$  combina-

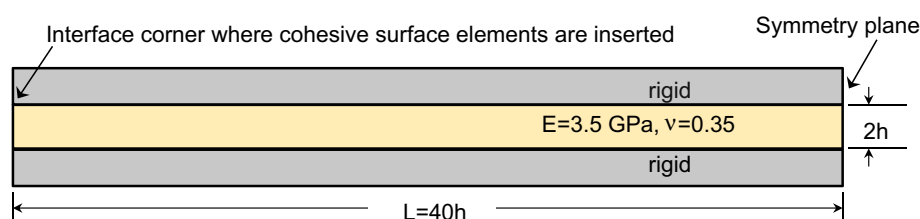


**Fig. 4.** Adhesively bonded butt joint model geometry where the bottom edge of the linear elastic adhesive layer is fixed while the top edge is displaced upwards.

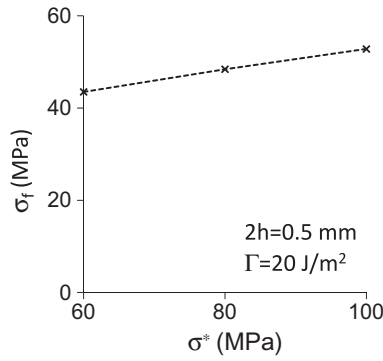


**Fig. 6.** Predicted butt joint strength  $\sigma_f$  when  $\Gamma$  is held fixed while  $\sigma^*$  is varied (used  $T$ - $U$  relationships in Fig. 5).

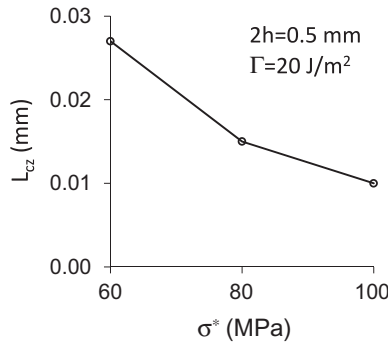


**Fig. 7.** Calculated CZ length  $L_{cz}$  when  $\Gamma$  is held fixed while  $\sigma^*$  is varied (used  $T$ - $U$  relationships in Fig. 5).

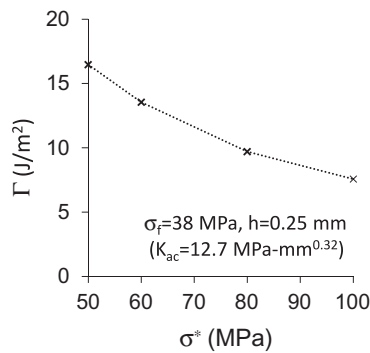


**Fig. 8.** Any number of  $\Gamma$ ,  $\sigma^*$  combinations produce the same value of  $K_{ac}$  (i.e., the same  $\sigma_f$  for a given  $2h$ ).

tions that predict the same joint strength for a layer of thickness  $2h$  (or alternately generate a fixed value of  $K_{ac}$ ). Fig. 8 plots results of four CZ fracture calculations, each using a different  $\Gamma$ ,  $\sigma^*$  combination, that predict that a butt joint with a 0.5 mm-thick adhesive layer fails at an applied tensile stress of 38 MPa (i.e., when  $K_{ac} = 12.7 \text{ MPa-mm}^{0.32}$ , a value that is consistent with the joint strength data plotted in Fig. 2). These  $\Gamma$ ,  $\sigma^*$  combinations were determined by trial and error (within 1% of targeted value) and each combination corresponds to a different  $L_{cz}$  (Fig. 9). Since there are any number of  $\Gamma$ ,  $\sigma^*$  combinations that generate the same joint strength, a  $T$ - $U$  relationship that successfully predicts butt joint failure cannot be considered to be a material-like property (since there are any number of  $T$ - $U$  relationships that would also successfully predict joint failure). In the next section, an approximate CZ-like elasticity solution is used to estimate  $\Gamma$ ,  $\sigma^*$  combinations that generate the same  $K_{ac}$ .

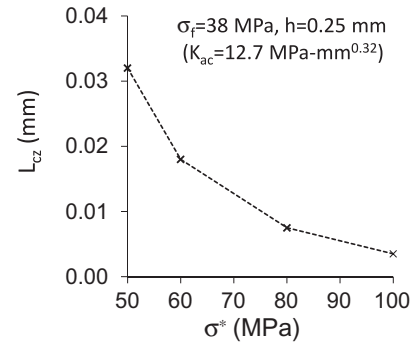


**Fig. 9.** Calculated CZ length  $L_{cz}$  for  $\Gamma$ ,  $\sigma^*$  combinations that produce the same value of  $K_{ac}$  ( $K_{ac} = 12.7 \text{ MPa-mm}^{0.32}$ ).

### 5. Approximate CZ-like elasticity solution for the case of a rectangular $T$ - $U$ relationship

An elasticity solution that provides insights into the connection between nominal joint strength  $\sigma_f$ , CZ parameters  $\Gamma$  and  $\sigma^*$ , and cohesive zone length  $L_{cz}$  is described in this section. The analysis is based on a simplified, approximate representation of the cohesive zone that emanates from the interface corner. Fig. 10 illustrates the nature of the tractions that are predicted by a CZ finite element analysis (CZ FEA) of an adhesively bonded butt joint when a rectangular  $T$ - $U$  is used (plotted results for the case where  $\sigma^* = 80 \text{ MPa}$  and  $\Gamma = 9.7 \text{ J/m}^2$ ). These results show that the normal traction  $T_n$  dominates within the CZ where  $T_n/T_t > 2.7$ . Hence,  $T_n$  is also a far greater contributor to the effective stress  $\sigma$ ,

$$\sigma = \sqrt{T_n^2 + T_t^2} \quad (6)$$

where  $\sigma$  is defined so as to be consistent with the Tvergaard and Hutchinson CZ model (i.e., derived using Eqs. (3) and (5)). Consequently, when constructing an approximate elasticity solution for a CZ embedded within the interface corner stress singularity, it seems reasonable to consider  $T_n$  as constant within the CZ. Although  $T_t$  varies more within the CZ, its relative magnitude is considerably less and consequently it also seems reasonable to also approximate it as constant within the CZ with this constant value representing the average value of  $T_t$ . Based upon these assumptions, a CZ-like elasticity solution for the case of a rectangular  $T$ - $U$  can be constructed by superimposing interfacial fracture solutions for: (1) a small interfacial edge crack of length  $a$  embedded within the interface corner's singular stress field (Fig. 11a), (2) a small interfacial edge-crack of length  $a$  loaded by a uniform crack-face pressure  $p^*$  (Fig. 11b), and (3) a small interfacial edge-crack edge of length  $a$

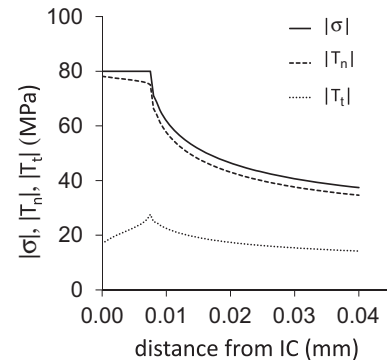


**Fig. 10.** Calculated interfacial normal  $T_n$  and shear  $T_t$  tractions as well as effective interfacial stress  $\sigma$  when a rectangular  $T$ - $U$  is used ( $\sigma^* = 80 \text{ MPa}$  and  $\Gamma = 9.7 \text{ J/m}^2$ ).

loaded by a uniform crack-face shear traction  $\tau^*$  (Fig. 11c). Furthermore, the approximate CZ-like solution, where  $a$  equals  $L_{CZ}$ , imposes the requirement that the sum of these three complex stress intensity factors equal zero (i.e., after superposition, the stress intensity factor at the crack tip vanishes). Each of these solutions will be presented next, followed by the approximate solution derived by their superposition. This analysis assumes that the adherends are rigid and that the CZ is embedded within the region dominated by the interface corner singularity. Also note that in this simplified, approximate representation of the cohesive zone, the CZ tractions  $T_n$  and  $T_t$  are not coupled in the same way as they are in the CZ FEA (i.e., in the CZ FEA  $T_n$  and  $T_t$  are coupled via Eqs. ((3)–(5)).

### 5.1. A small interfacial edge-crack embedded within the interface corner's singular stress field

The solution to this problem has been published previously (Reedy, 2000). A short, interfacial crack is considered to be fully embedded within the region dominated by the interface corner stress singularity (Fig. 11a). The angular variation of displacements along the outer boundary (radial distance from the interface corner  $r \gg a$ ) is known from the interface corner solution (Fig. 1), and  $K_a$  determines the magnitude of the loading. A dimensional analysis indicates that the complex stress intensity  $K_{ssc}$  for this small-scale cracking problem can be expressed in terms of problem parameters as

$$K_{ssc} = K_a a^{(2\lambda-1)/2} D(\nu)^{1/2} e^{i\psi_{r=a}^{ssc}} \quad (7)$$

where  $K_a$  is defined by Eq. (1). The function  $D(\nu)$  and the phase angle  $\psi_{r=a}^{ssc}$  (evaluated at a characteristic distance  $a$  in front of the crack-tip) are determined for  $\nu$  values of interest by matching Eq. (7) with finite element results for the same asymptotic problem. When  $\nu = 0.35$ ,  $D = 5.89$  and  $\psi_{r=a}^{ssc} = -16.5^\circ$  (recall from the discussion of the IC solution in Section 2, when  $\nu = 0.35$ ,  $1 - \lambda = 0.320$ , and  $A = 0.958$ ). Based on dimensional considerations, the normal and tangential crack flank displacements at the stress-free edge,  $\delta_n^{ssc}$  and  $\delta_t^{ssc}$ , respectively, can be expressed as

$$\delta_n^{ssc} = K_a a^2 f_n(\nu) / E^* \quad (8)$$

$$\delta_t^{ssc} = K_a a^2 f_t(\nu) / E^* \quad (9)$$

where

$$E^* = 2E / (1 - \nu^2) \quad (10)$$

When  $\nu = 0.35$ ,  $f_n = 7.57$  and  $f_t = -0.41$ .

### 5.2. A small pressurized interfacial edge crack

A dimensional analysis indicates that the complex stress intensity  $K_p$  for the asymptotic problem of a small interfacial edge-crack of length  $a$  loaded by a crack-face pressure  $p^*$  (Fig. 11b) can be expressed in terms of problem parameters as

$$K_p = p^* (\pi a b(\nu))^{1/2} e^{i\psi_{r=a}^p} \quad (11)$$

The function  $b(\nu)$  and the phase angle  $\psi_{r=a}^p$  are determined for  $\nu$  values of interest by matching Eq. (11) with finite element results for the same asymptotic problem. When  $\nu = 0.35$ ,  $b = 1.132$  and  $\psi_{r=a}^p = 0.6^\circ$ . The normal and tangential crack flank displacements at the stress-free edge,  $\delta_n^p$  and  $\delta_t^p$ , respectively, can be expressed as

$$\delta_n^p = p^* a d_n(\nu) / E^* \quad (12)$$

$$\delta_t^p = p^* a d_t(\nu) / E^* \quad (13)$$

When  $\nu = 0.35$ ,  $d_n = 4.91$  and  $d_t = 1.42$ .

### 5.3. A small interfacial edge-crack with a crack-face shear traction

A dimensional analysis indicates that the complex stress intensity  $K_t$  for the asymptotic problem of a small interfacial edge-crack of length  $a$  loaded by a crack-face shear traction  $\tau^*$  (Fig. 11c) can be expressed in terms of problem parameters as

$$K_t = t^* (\pi a c(\nu))^{1/2} e^{i\psi_{r=a}^t} \quad (14)$$

The function  $c(\nu)$  and the phase angle  $\psi_{r=a}^t$  are determined for  $\nu$  values of interest by matching Eq. (14) with finite element results for the same asymptotic problem. When  $\nu = 0.35$ ,  $c = 1.305$  and  $\psi_{r=a}^t = -104.5^\circ$ . The normal and tangential crack flank displacements at the stress-free edge,  $\delta_n^t$  and  $\delta_t^t$ , respectively, can be expressed as

$$\delta_n^t = t^* a e_n(\nu) / E^* \quad (15)$$

$$\delta_t^t = t^* a e_t(\nu) / E^* \quad (16)$$

When  $\nu = 0.35$ ,  $e_n = -3.47$  and  $e_t = -5.58$ .

### 5.4. Approximate CZ-like solution for an adhesively bonded butt joint

A CZ-like elasticity solution for the case of a rectangular T-U is constructed by superimposing the three interfacial fracture solutions presented above in Sections 5.1–5.3 along with the requirement that the sum of the their associated complex stress intensities factors equal zero (there is no stress singularity at the tip of the CZ). Accordingly,

$$K_{ssc} + K_p + K_t = 0 \quad (17)$$

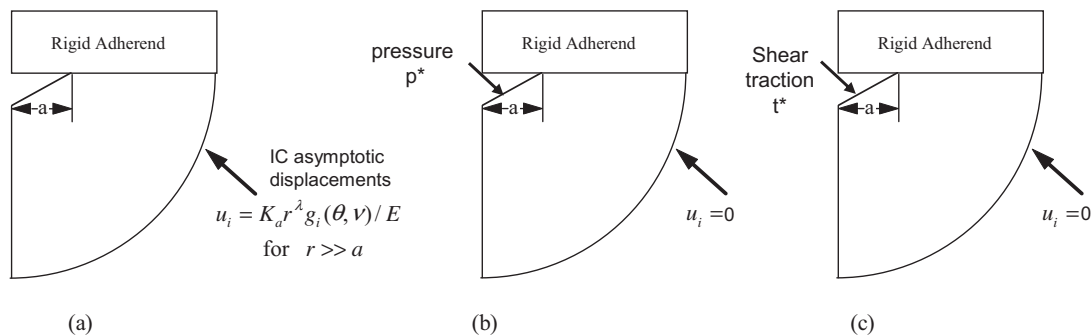


Fig. 11. Three asymptotic problems used to construct a CZ-like solution for a sharp-edged butt joint: (a) interfacial edge crack embedded within the interface corner's singular stress field, (b) uniform pressure applied to a small interfacial edge-crack, and (c) uniform shear traction applied to surface of a small interfacial edge-crack.

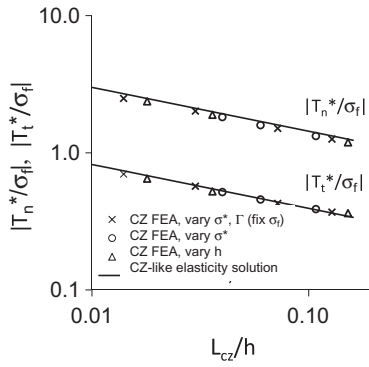


Fig. 12. Comparison of interfacial tractions predicted by CZ FEA with those predicted by an approximate CZ-like elasticity solution.

where the complex stress intensity factors are defined by Eqs. (7), (11) and (14). The set of equations generated by setting the real and imaginary parts of Eq. (17) to zero can be solved for  $p^*$  and  $t^*$ . When  $\nu = 0.35$ ,

$$p^*/\sigma_f = -0.687(a/h)^{-0.320} \quad (18)$$

$$t^*/\sigma_f = -0.188(a/h)^{-0.320} \quad (19)$$

Note that crack length  $a$  corresponds to the length of the CZ  $L_{cz}$ . To enable a comparison to CZ FEA results, an effective interfacial stress is defined in terms of the interfacial tractions in the CZ-like solution ( $p^*$  corresponds to  $T_n$  and  $t^*$  corresponds to  $T_t$  in Eq. (6)). Consequently, the normalized effective stress within the CZ is defined as

$$\sigma^*/\sigma_f = \left( (p^*/\sigma_f)^2 + (t^*/\sigma_f)^2 \right)^{1/2} \quad (20)$$

When  $\nu = 0.35$  (using Eqs. (18) and (19)),

$$\sigma^*/\sigma_f = 0.712(a/h)^{-0.320} \quad (21)$$

The CZ-like elasticity solution can also be used to estimate the normal and tangential crack flank displacements at the stress-free edge. The total crack flank edge displacements are determined by summing the individual contributions from each of the superimposed solutions (summing Eqs. (8), (12) and (15) and also (9), (13) and (16)). When  $\nu = 0.35$  (using Eqs. (18) and (19)),

$$\delta_n/h = (\delta_n^{ssc} + \delta_n^p + \delta_n^t)/h = 0.519(\sigma_f/E)(a/h)^{0.680} \quad (22)$$

$$\delta_t/h = (\delta_t^{ssc} + \delta_t^p + \delta_t^t)/h = -0.061(\sigma_f/E)(a/h)^{0.680} \quad (23)$$

An effective  $\delta$  can also be defined in a way that is consistent with the effective separation used in the Tvergaard and Hutchinson CZ model (Eq. (3)), and for  $\nu = 0.35$

$$\delta/h = \left( (\delta_n/h)^2 + (\delta_t/h)^2 \right)^{1/2} = 0.523(\sigma_f/E)(a/h)^{0.680} \quad (24)$$

Finally, the CZ-like elasticity solution is used to define a work of separation/unit area-like quantity that can be compared to CZ FEA results. Specifically, this analogue to the work of separation is defined as the product of the effective stress in the CZ (Eq. (21)) and the effective crack flank displacement (Eq. (24)). When  $\nu = 0.35$ , the nondimensionalized analogue to the work of separation/unit area is

$$(E\Gamma)/(\sigma_f^2 h) = 0.372(a/h)^{0.360} \quad (25)$$

### 5.5. Comparison of CZ-like elasticity solution with CZ finite element results

Fig. 12 compares the interfacial tractions within the CZ that are predicted by a finite element CZ failure analysis with those predicted by the approximate CZ-like elasticity solution (normalized by  $\sigma_f$ ) as a function of CZ length (normalized by  $h$ ). The results of the CZ-like elasticity solution are defined by Eqs. (18) and (19) (note that  $a$ ,  $p^*$ , and  $t^*$  correspond to  $L_{cz}$ ,  $T_n^*$ , and  $T_t^*$ , respectively, where  $T_n^*$  and  $T_t^*$  are interfacial tractions within the CZ). Three sets of finite element results are also plotted (a different symbol is used for each set): (1) analyses where  $\sigma^*$  and  $\Gamma$  are varied while maintaining  $\sigma_f = 38$  MPa and  $2h = 0.5$  mm (results of these calculations are also plotted in Figs. 8 and 9), (2) analyses where  $\sigma^*$  is varied while maintaining  $2h = 0.5$  mm and  $\Gamma = 20$  J/m<sup>2</sup> (results of these calculations are also plotted in Figs. 6 and 7), and (3) analyses where  $2h$  is varied while maintaining  $\sigma^* = 60$  MPa and  $\Gamma = 13.5$  J/m<sup>2</sup> (results of these calculations are also plotted in Fig. 18). Since the  $T_n^*$  and  $T_t^*$  values calculated by the CZ FEA vary somewhat within the CZ (Fig. 10), their value at the mid-point of the CZ is used in the comparison. The agreement between the CZ-like elasticity solution and the CZ finite element failure analysis is quite good. The CZ tractions that were determined from the finite element analysis follow the power-law relationship as predicted by the CZ-like elasticity solution (Eqs. (18) and (19)). The magnitude of the tractions varies in a predictable way with the length of the CZ.

Figs. 13 and 14 plot the CZ-like elasticity relationships defined by Eqs. (21) and (25), respectively. Collectively, these results can be used to identify  $\sigma^*$ ,  $\Gamma$  pairs that when used in a CZ FEA will generate a predicted butt joint strength equal to  $\sigma_f$  when the corresponding bond thickness is  $2h$  (plotted results for  $\nu = 0.35$ ). There are any number of possible  $\sigma^*$ ,  $\Gamma$  combinations, each corresponding to a different  $L_{cz}/h$ . The agreement between the CZ FEA results and the CZ-like elasticity solution is very good (Figs. 13 and 14) and predicted relationships follow the expected power-law behavior with exponents of  $-0.32$  and  $0.36$ , respectively (Eqs. (21) and (25)). The approximate CZ-like elasticity solution explains why the particular  $\sigma^*$ ,  $\Gamma$  choices plotted in Fig. 8, which was determined by trial and error, all predict the same joint strength  $\sigma_f$ . The interfacial tractions within the CZ produce a complex  $K$  that cancels that found at tip of a crack of the same length as the CZ. There is a different solution for each CZ length.

Finally, note that Eqs. (21) and (25) can be solved so as to remove their mutual dependency on  $\sigma_f$

$$\frac{E\Gamma}{\sigma_f^2 L_{cz}} = 0.734 \quad (26)$$

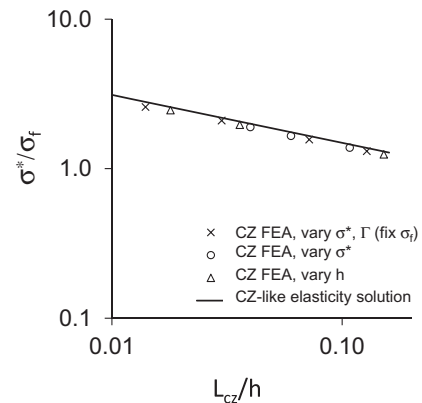
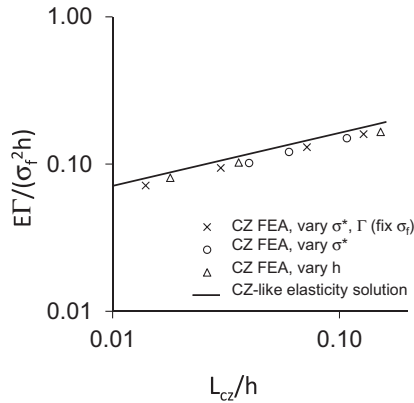
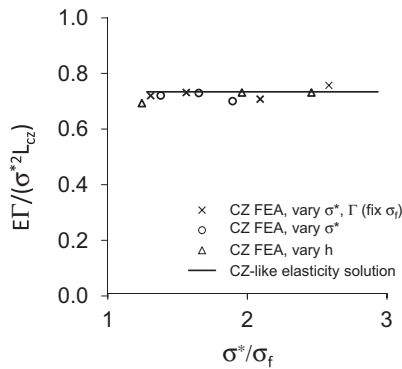


Fig. 13. Comparison of relationship between  $\sigma^*/\sigma_f$  and  $L_{cz}/h$  as predicted by a CZ FEA with that predicted by an approximate CZ-like elasticity solution.



**Fig. 14.** Comparison of relationship between  $EI\Gamma/(\sigma_f^2 h)$  and  $L_{cz}/h$  as predicted by a CZ FEA with that predicted by an approximate CZ-like elasticity solution.



**Fig. 15.** The value of the nondimensional parameter  $EI\Gamma/(\sigma_f^2 L_{cz})$  as computed from finite element results is nearly constant and agrees with the CZ-like elasticity solution.

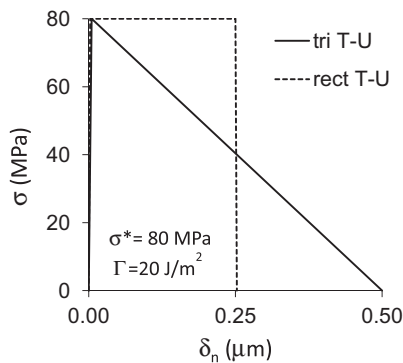


**Fig. 16.**  $T$ – $U$  relationship used in calculations where  $\Gamma$  and  $\sigma^*$  are held fixed, but the shape is either triangular (tri) or rectangular (rect); shown for the case of a pure mode I loading.

This result shows that there is a nondimensional parameter, as defined by the left hand side of Eq. (26), that directly relates the CZ parameters  $\Gamma$ ,  $\sigma^*$ , and  $L_{cz}$  (along with layer  $E$ ) that is independent of the specific joint failure load and bond thickness. The value of this nondimensional quantity depends only on the Poisson's ratio (the Eq. (26) result is for  $\nu = 0.35$ ). The values of  $\sigma_f$  and  $h$  (or  $K_{ac}$ ) for a particular choice of the CZ parameters is not immediately apparent, but can be determined using Eqs. (21) and (26). The value of this nondimensional quantity was computed using the same FEA results as used in constructing Figs. 13 and 14. Fig. 15 shows that

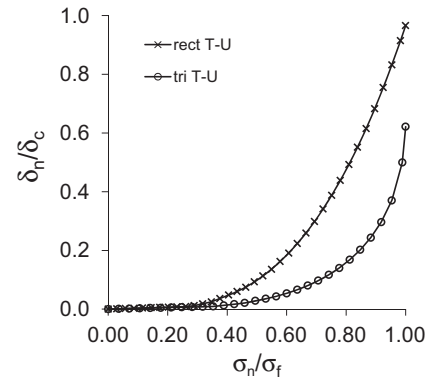


**Fig. 17.** Comparison of normalized opening at the root of the CZ as a function of the normalized applied load for the rectangular and triangular  $T$ – $U$  relationships shown in Fig. 16 ( $\Gamma$  and  $\sigma^*$  are held fixed).

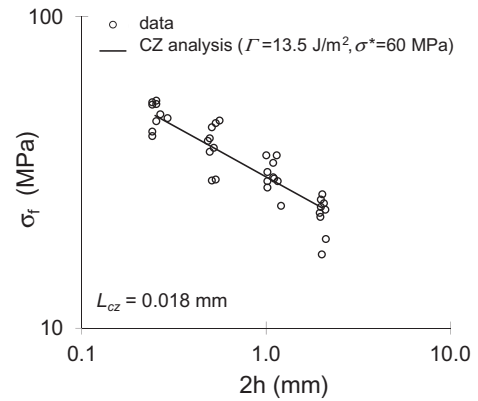


**Fig. 18.** Comparison of measured butt joint tensile strength vs. bond thickness data with prediction based on a CZ finite element analysis.

the computed value of this nondimensional parameter is approximately constant and its value is in good agreement with the CZ-like elasticity solution.

## 6. Comparison of CZ FEA that use triangular and rectangular $T$ – $U$ relationships with same $\Gamma$ and $\sigma^*$

Although this study is focused primarily on how changing the aspect ratio of a rectangular  $T$ – $U$  relationship affects the predicted butt joint strength, a limited number of calculations also examined how the predicted joint strength depends on the choice of a rectangular vs. triangular  $T$ – $U$  relationship. Fig. 16 shows the rectangular (rect) and the triangular (tri)  $T$ – $U$  relationships that were used in the CZ calculations discussed in this section. Both of these relationships have the same values of  $\sigma^*$  and  $\Gamma$  ( $\sigma^* = 80$  MPa, and  $\Gamma = 20$  J/m<sup>2</sup>). Table 1 indicates that the predicted value of  $\sigma_f$  is 20% greater when the rectangular  $T$ – $U$  relationship is used. Table 1 also indicates that the predicted strength does not change appreciably with mesh refinement.

In the calculation that used the rectangular  $T$ – $U$  relationship, the CZ was fully developed when the crack begins to propagate (i.e.,  $\chi = 1$  at root of the CZ). This was also true for all the other calculations presented in this paper (they all used a rectangular  $T$ – $U$  relationship). Furthermore, the CZ-like solution does not exclude any choice of cohesive zone parameters. This suggests that a CZ FEA that uses a rectangular  $T$ – $U$  can determine a solution with a fully developed cohesive zone for any choice of cohesive zone parameters (provided that small scale yielding-like conditions

apply in the rigid adherend, adhesively bonded butt joint). In contrast, it appears that an apparent instability occurred in the calculation where the triangular  $T$ – $U$  was used. Fig. 17 compares the normal opening at the interface corner (normalized by the critical opening  $\delta_c$  for the respective  $T$ – $U$  relationships) as a function of the normalized applied tensile stress  $\sigma_n/\sigma_f$ . The opening at the root of the CZ displays an apparent limit-like response as  $\sigma_n/\sigma_f$  approaches one when the triangular  $T$ – $U$  relationship is used. It is well known that numerical instabilities can arise when the stiffness of the adjoining bulk elements is relatively low compared to the triangular  $T$ – $U$ 's unloading stiffness (Foulk, 2010). However, this is not the source of the instability observed here since the element stiffness was more than an order of magnitude greater than that, triangular  $T$ – $U$ 's unloading stiffness in this calculation.

The calculations for the rectangular and triangular  $T$ – $U$  relationships were repeated using an explicit dynamics finite element code so as to roughly estimate when rapid crack growth commences. This is done by loading the specimen to a specified edge displacement (or equivalently a specified  $\sigma_n$ ) and then holding this displacement fixed to determine if the interface separates without further loading. For the case of the triangular  $T$ – $U$ , the cohesive zone did not extend during the hold when the specimen was loaded to level such that the maximum effective separation at the root of the cohesive zone  $\chi$  equaled 0.49 ( $\chi$  defined in Eq. (3)). However, when the load level was increased by about 1% and the maximum value of  $\chi$  was 0.56, the cohesive zone continued to grow while the load was fixed, and ultimately  $\chi$  equaled 1.00 and the interface separated as crack grew from the interface corner. In contrast the cohesive zone did not extend when the rectangular  $T$ – $U$  relationship was used even when the maximum value of  $\chi$  equaled 0.95 at the beginning of the hold. This strongly suggests that a dynamic instability occurred before the CZ was fully developed when the triangular  $T$ – $U$  was used. It would seem that in this particular analysis the relatively rapid rise in the energy release rate as the length of a small crack increases overwhelms the incremental increase in the resistance associated with the tail of the triangular  $T$ – $U$  relationship. This is a topic that deserves further attention. There is no reason to believe that all triangular  $T$ – $U$  relationships will produce the sort of instability depicted in Fig. 17. Additional work is needed to define the nature of this instability and its relationship to the parameters that define the shape of the  $T$ – $U$  relationship.

It has been noted by others that a rectangular  $T$ – $U$  relationship seemed to work better than other shapes when analyzing the initiation of crack growth from a sharp notch (Gomez and Ellices, 2003). It is possible that some  $T$ – $U$  relationships with non-rectangular shapes are more prone to a dynamic instability and this explains their poorer performance. This is potentially an important consideration when applying a CZ fracture analysis to predict the initiation of crack growth from material and geometric discontinuities other than a long preexisting crack.

## 7. Discussion

The predicted strength of a rigid adherend, adhesively bonded butt joint was found to depend on the shape of the  $T$ – $U$  relationship used in the CZ fracture analysis. There was no preexisting crack in the problem analyzed and the CZ was small compared to the thickness of the elastic layer (small scale yielding-like conditions applied). The predicted dependence on the shape of the  $T$ – $U$  relationship can be contrasted to the case of a long, preexisting crack between elastic materials where a CZ analysis will yield a failure prediction that depends only on the work of separation/unit area (fracture toughness) provided that the CZ is sufficiently small. Most of the CZ calculations reported herein used a rectangular  $T$ – $U$

relationship, and this relationship is defined by two parameters: the interfacial strength  $\sigma^*$  and the work of separation/unit area  $\Gamma$ . The primary finding of this study is that for a specified adhesive layer thickness, there is any number of  $\sigma^*$ ,  $\Gamma$  combinations that generate the same predicted joint strength. Each combination corresponds to a different CZ length. An approximate CZ-like elasticity solution was developed to show how such combinations arise.

In some sense, the CZ can be considered to be the “initial flaw” when there is no preexisting crack and, consequently, the shape of the  $T$ – $U$  relationship matters since it controls the CZ length as well as the magnitude and distribution of CZ tractions. Since there are any number of  $\Gamma$ ,  $\sigma^*$  combinations that generate the same joint strength, a  $T$ – $U$  relationship that simply predicts the measured butt joint failure load cannot be considered to be a material-like property.

It is important to note that any of the  $\Gamma$ ,  $\sigma^*$  combinations that predicts the strength of a butt joint at one bond thickness can successfully predict the strength at other bond thicknesses. This should be true provided that the CZ is deeply embedded with the interface corner  $K_a$  field and small scale yielding-like conditions apply. Consequently, identifying one particular  $\Gamma$ ,  $\sigma^*$  combination that successfully predicts the dependence of joint strength on bond thickness does not mean that that combination has special significance. The ability to predict the dependence of joint strength on bond thickness is illustrated in Fig. 18. The  $\Gamma$ ,  $\sigma^*$  combination  $\Gamma = 13.5 \text{ J/m}^2$  and  $\sigma^* = 60$  is one of any number of  $\Gamma$ ,  $\sigma^*$  combinations that predict the strength of an adhesive layer with  $2h = 0.5$  to be 38 MPa (see Fig. 8). Note that this choice of joint strength matches that measured in experiments where  $2h = 0.5$  (Fig. 2). Using this  $\Gamma$ ,  $\sigma^*$  combination, the strength of joints with  $2h = 0.25, 0.5, 1.0$ , and  $2.0 \text{ mm}$  were predicted by a CZ analysis and those results were used to define the  $\sigma_f$  vs.  $2h$  relationship plotted in Fig. 18. Also plotted in Fig. 18 is the experimental data previously plotted in Fig. 2. The CZ calculation predicts the dependence of joint tensile strength on adhesive layer thickness.

Although the results presented here are for the particular case of an idealized, adhesively bonded butt joint, they are expected to have broader applicability. Specifically, the shape of the CZ model may potentially affect the predicted response whenever a CZ fracture analysis is used to predict the initiation of crack growth from material and geometric discontinuities other than that of a long preexisting crack. Even though a CZ FEA successfully predicts a joint's measured fracture strength, the parameters defining the  $T$ – $U$  relationship used in that analysis may have limited physical significance. There is presumably any number of  $T$ – $U$  relationships that would also successfully predict failure.

## Acknowledgment

This work was supported by the Laboratory Directed Research and Development Program at Sandia National Laboratories. Sandia National Laboratories is a multi-program laboratory managed and operated by Sandia Corporation, a wholly owned subsidiary of Lockheed Martin Corporation, for the US Department of Energy's National Nuclear Security Administration under contract DE-AC04-94AL85000.

## References

- Banea, M.D., da Silva, L.F.M., 2009. Adhesively bonded joints in composite materials: an overview. *Proc. Inst. Mech. Eng. L-J. Mater. Des. Appl.* 223 (L1), 1–18.
- Blackman, B.R.K., Hadavinia, H., Kinloch, A.J., Williams, J.G., 2003. The use of a cohesive zone model to study the fracture of fibre composites and adhesively-bonded joints. *Int. J. Fract.* 119 (1), 25–46.
- Foulk III, J.W., 2010. An examination of stability in cohesive zone modeling. *Comput. Methods Appl. Mech. Eng.* 199, 465–470.
- Gomez, F.J., Ellices, M., 2003. Fracture of components with V-shaped notches. *Eng. Fract. Mech.* 70 (14), 1913–1927.

- Gustafson, P.A., Waas, A.M., 2009. The influence of adhesive constitutive parameters in cohesive zone finite element models of adhesively bonded joints. *Int. J. Solids Struct.* 46 (10), 2201–2215.
- Kafkalidis, M.S., Thouless, M.D., 2002. The effects of geometry and material properties on the fracture of single lap-shear joints. *Int. J. Solids Struct.* 39 (17), 4367–4383.
- Liljedahl, C.D.M., Crocombe, A.D., Wahab, M.A., Ashcroft, I.A., 2006. Damage modelling of adhesively bonded joints. *Int. J. Fract.* 141 (1–2), 147–161.
- Mohammed, I., Liechti, K.M., 2000. Cohesive zone modeling of crack nucleation at bimaterial corners. *J. Mech. Phys. Solids* 48 (4), 735–764.
- Reedy Jr., E.D., 1990. Intensity of the stress singularity at the interface corner between a bonded elastic and rigid layer. *Eng. Fract. Mech.* 36, 575–583.
- Reedy Jr., E.D., 1993. Asymptotic interface corner solutions for butt tensile joints. *Int. J. Solids Struct.* 30, 767–777.
- Reedy Jr., E.D., 2000. Connection between interface corner and interfacial fracture analyses of an adhesively bonded butt joint. *Int. J. Solids Struct.* 37, 2429–2442.
- Reedy Jr., E.D., Guess, T.R., 1993. Comparison of butt tensile strength data with interface corner stress intensity factor prediction. *Int. J. Solids Struct.* 30, 2929–2936.
- Reedy Jr., E.D., Guess, T.R., 1997. Interface corner failure analysis of joint strength: effect of adherend stiffness. *Int. J. Fract.* 88, 305–314.
- Reedy Jr., E.D., Guess, T.R., 1999. Additional interface corner toughness data for an adhesively-bonded butt joint. *Int. J. Fract.* 98, L3–L8.
- Thomas, J.D., 2011. *Sierra/SolidMechanics 4.22 User's Guide*, SAND2011-7597. SIERRA Solid Mechanics Team Albuquerque, Sandia National Laboratories.
- Tvergaard, V., Hutchinson, J.W., 1993. The influence of plasticity on mixed mode interface toughness. *J. Mech. Phys. Solids* 41, 1119–1135.
- Xu, X.-P., Needleman, A., 1994. Numerical simulations of fast crack growth in brittle solids. *J. Mech. Phys. Solids* 42, 1397–1434.
- Yang, Q.D., Thouless, M.D., 2001. Mixed-mode fracture analyses of plastically-deforming adhesive joints. *Int. J. Fract.* 110 (2), 175–187.